The Astronomical Journal, 135:1430–1440, 2008 April doi:10.1088/0004-6256/135/4/1430

A NEW VLA–*HIPPARCOS* DISTANCE TO BETELGEUSE AND ITS IMPLICATIONS

Graham M. Harper[1], Alexander Brown[1], and Edward F. Guinan[2]
[1] Center for Astrophysics and Space Astronomy, University of Colorado, Boulder, CO 80309, USA; graham.harper@colorado.edu, alexander.brown@colorado.edu
[2] Department of Astronomy and Astrophysics, Villanova University, PA 19085, USA; edward.guinan@villanova.edu
Received 2007 November 2; accepted 2008 February 8; published 2008 March 10

ABSTRACT

The distance to the M supergiant Betelgeuse is poorly known, with the *Hipparcos* parallax having a significant uncertainty. For detailed numerical studies of M supergiant atmospheres and winds, accurate distances are a prerequisite to obtaining reliable estimates for many stellar parameters. New high spatial resolution, multiwavelength, NRAO[3] Very Large Array (VLA) radio positions of Betelgeuse have been obtained and then combined with *Hipparcos* Catalogue Intermediate Astrometric Data to derive new astrometric solutions. These new solutions indicate a smaller parallax, and hence greater distance (197 ± 45 pc), than that given in the original *Hipparcos* Catalogue (131 ± 30 pc) and in the revised *Hipparcos* reduction. They also confirm smaller proper motions in both right ascension and declination, as found by previous radio observations. We examine the consequences of the revised astrometric solution on Betelgeuse's interaction with its local environment, on its stellar properties, and its kinematics. We find that the most likely star-formation scenario for Betelgeuse is that it is a runaway star from the Ori OB1 association and was originally a member of a high-mass multiple system within Ori OB1a.

Key words: astrometry – radio continuum: stars – stars: individual (α Ori) – stars: kinematics – supergiants – techniques: interferometric

1. INTRODUCTION

The study of stellar activity, and in particular mass loss, involves a combination of detailed numerical studies of individual stars together with broader surveys of similar stars that measure a variety of atmospheric diagnostics. To gain physical insight, quantitative studies require accurate stellar parameters: for example, the distance leads to the luminosity and when combined with an angular diameter gives the physical radius and effective temperature; luminosity and isotopic abundances provide estimates of the stellar age and mass. Except for ζ Aurigae eclipsing binary systems, e.g., Bennett et al. (1996) and Harper et al. (2005), accurate stellar parameters for cool supergiants are not available.

The M supergiant Betelgeuse (α Orionis, HD 39801, HIP 27989) is bright, has a large wavelength-dependent angular diameter, and has been the subject of many observational, theoretical and modeling efforts. However, its distance and therefore most of its other parameters are not well determined. Prior to the *Hipparcos* Catalogue the most up-to-date published parallax for Betelgeuse was $\pi = 9.8 \pm 4.7$ mas ($d \sim 102$ pc) from the Fourth Edition of the Yale Trigonometric Parallaxes (van Altena et al. 1995), while the *Hipparcos* Input Catalogue, Version 2 (ESA 1993) gives a trigonometric parallax of $\pi = 5 \pm 4$ mas ($d \sim 200$ pc). A summary of pre-*Hipparcos* stellar motions and parallax is given in Table 1. The significance of the *Hipparcos* parallax is not sufficient to derive the distance or stellar peculiar velocity with confidence, and a wide range of distance estimates have also been adopted by researchers. For example, White (1980) used a CN index to derive M_v which, with a visual extinction of $A_v = 0.7$, gave a photometric distance of 96 pc, and Lambert et al. (1984) combined a mean apparent magnitude of $m_v = 0.8$ and $A_v = 0.7$ with an assumed $M_v = -5.85$ to derive a distance of 155 pc, noting that a range of $0.3 < A_v < 0.8$ was likely. A value of 400 pc was invoked by Knapp & Morris (1985) to explain a discrepancy between their circumstellar CO observations and models. This extreme distance would imply that Betelgeuse is overluminous for its spectral type (Huggins 1987), and this distance can likely be discounted as independent observations of C I now indicate that CO is not fully associated in the stellar wind (Huggins et al. 1994).

The *Hipparcos* Catalogue (ESA 1997) provided a great improvement in the distance estimates for many nearby stars that have been studied in detail spectroscopically at multiple wavelengths, and have interferometric angular diameters (e.g., van Belle et al. 1999; Mozurkewich et al. 2003). Unfortunately, the *Hipparcos* astrometric solution for Betelgeuse (given in Table 2) has significant uncertainties in both the parallax and proper motions.[4]

In angular units (mas), following the *Hipparcos* nomenclature, the uncertainties in R.A., the proper motion in R.A., and the uncertainty in the proper motion are indicated by $\Delta(\alpha \cos\delta)$, $\mu_{\alpha \cos\delta}$, and $\Delta(\mu_{\alpha \cos\delta})$, respectively. The *Hipparcos* solution for Betelgeuse is a stochastic solution of type X (*Hipparcos* Catalogue: Section 2.3.6). The normal single star 5-parameter solution was found to be unsatisfactory because the χ^2 was larger than expected based on the predicted measurement standard errors. The *Hipparcos* astrometric solution is derived from 1D position measurements (abscissae) of meridians whose positions are accurately known—the position of the star along the individual meridians, however, is not well known. The astrometric solution is found by fitting astrometric models to these abscissae. A detailed discussion is given in van Leeuwen & Evans (1998).

In the case of Betelgeuse an additional error (noise) term was added in quadrature (stochastic solution type X) to the *abscissa*

[3] The National Radio Astronomy Observatory is a facility of the National Science Foundation operated under cooperative agreement by Associated Universities, Inc.

[4] The five astrometric parameters are: right ascension (R.A.) = α; declination (decl.) = δ; parallax= π; proper motion in R.A. = μ_α, and proper motion in decl. = μ_δ.

Table 1
Pre-*Hipparcos* Proper Motions and Parallax, and the Stellar Radial Velocity

Parameter	Value	Uncertainty	Units	Source
$\mu_{\alpha\cos\delta}$	25.73	0.30	mas yr^{-1}	FK5 (J2000.0); Fricke et al. (1988)
μ_δ	8.7	0.33	mas yr^{-1}	FK5 (J2000.0); Fricke et al. (1988)
π	9.8	4.7	mas	van Altena et al. (1995)
$v_{\rm rad}$	+20.7	0.4	km s^{-1} (heliocentric)	Sanford (1933); Jones (1928)

Table 2
Hipparcos Astrometric Solution: ICRS Epoch 1991.25

Parameter	Value	Units	Error	Units	Comment
α	88.79287161	deg	1.51	mas	error in $\alpha\cos\delta$
δ	7.40703634	deg	1.13	mas	error in δ
Parallax π	7.63	mas	1.64	mas	131 ± 30 pc
$\mu_{\alpha\cos\delta}$	27.33	mas yr^{-1}	2.30	mas yr^{-1}	
μ_δ	10.86	mas yr^{-1}	1.46	mas yr^{-1}	
Cosmic error	3.36	mas	0.62	mas	stochastic type-X

Table 3
Betelgeuse Proper Motions

Parameter	Value (mas yr^{-1})	Uncertainty (mas yr^{-1})	Source
$\mu_{\alpha\cos\delta}$	27.33	2.30	*Hipparcos*; ESA (1997)
μ_δ	10.86	1.46	*Hipparcos*; ESA (1997)
$\mu_{\alpha\cos\delta}$	25.0	0.4	FK5 Rotated to *Hipparcos* 1151 stars
μ_δ	9.0	0.4	FK5 Rotated to *Hipparcos* 1151 stars
$\mu_{\alpha\cos\delta}$	23.98	1.04	VLA ICRF; Boboltz et al. (2007)
μ_δ	10.07	1.15	VLA ICRF; Boboltz et al. (2007)

errors, σ, i.e.,

$$\sigma' = \sqrt{\sigma^2 + \epsilon^2},$$

where ϵ is referred to as the *cosmic error*. The value of the cosmic error adopted is that required so that the reduced $\chi^2 \simeq 1$ and hence reflects the excess noise in the solution and *may* be related to the positional movement of the stellar photocenter. For Betelgeuse the mean of the abscissa standard errors is 2.2 mas, whereas the additional cosmic error is 3.36 ± 0.62 mas (*Hipparcos* Catalogue: Double and Multiple Systems Annex). These larger errors lead to larger uncertainty in the parallax than might otherwise have been expected. The origin of this cosmic error, whether it is stellar (photocenter motions on short timescales) or instrumental (resulting from large bright sources), is under investigation,[5] but has yet to be understood.

Prior to *Hipparcos*, accurate proper motions were available from the Fifth Fundamental Catalogue FK5 (Fricke et al. 1988) (see Table 1). The formal errors on these proper motions are much smaller ($\simeq$0.3 mas yr^{-1}) than those given in the *Hipparcos* Catalogue ($\sim$2 mas yr^{-1}). The *Hipparcos* positions and proper motions are tied to the International Celestial Reference System (ICRS) through a link between the *Hipparcos* Reference Frame and the ICRS with an uncertainty in the link of 0.6 mas in the alignment of the axes (at J1991.25) and 0.25 mas yr^{-1} in the relative rotation of the systems (*Hipparcos* Catalogue: Section 1.2.2). The FK5 and *Hipparcos* catalogs are not tied to each other so that reference frame rotations between FK5 and the *Hipparcos* realization of ICRS must be considered before the proper motions can directly be compared. The required angular rotation rates have been obtained by comparing FK5 and *Hipparcos* proper motions for significant stellar samples, e.g., Mignard & Froeschlé (2000), Schwan (2001), and Walter & Hering (2005). The internal errors on these derived rotations are $\simeq$0.1 mas and we can convert Betelgeuse's FK5 proper motions into the *Hipparcos* frame using Equations (7) and (8), and the 1151 star rotation rates given in Walter & Hering (2005).[6] The rotated proper motions are given in Table 3 and are smaller than the *Hipparcos* values. Positions of Betelgeuse also have been measured at radio wavelengths with the NRAO Very Large Array (VLA) and these measurements use phase (position) calibrators whose positions are accurately known in the International Celestial Reference Frame (ICRF) (Boboltz et al. 2007). The derived VLA proper motions are also given in Table 3 and suggest that the proper motions in R.A. and decl. are overestimated by *Hipparcos* and therefore the *Hipparcos* astrometric solution is not optimal. While these independent proper motions are significantly different from the nominal *Hipparcos* values, the large *Hipparcos* uncertainties do not invalidate its astrometric solution.

Fortunately, the *Hipparcos* Catalogue also contains Intermediate Astrometric Data that provide the means to improve and revise the astrometric solution when other measurements, such as radio measurements, are available (van Leeuwen & Evans 1998). We have been undertaking a detailed multi-wavelength and temporal study of the shape and brightness of Betelgeuse's

[5] C. Babusiaux & A. Jorissen, presentation at the 4th Gaia Variable Star Working Group (July 2005).

[6] Walter & Hering (2005) also point out that the rotation rates can differ at the 1 mas level in extreme cases depending on position with those expected from the luni-solar precession correction; so additional systematic errors may be present.

Table 4
Radio Positions of Phase Calibrators, and their separation from Betelgeuse (From the Current VLBA Phase Calibrator List)

IAU name	VLA calibrator name (J2000)	R.A. (J2000)	Decl. (J2000)	Position error (mas)	Reference	Separation (deg)
J0532+0732	0532+075	05 32 38.998475	07 32 43.34547	1.06	Ma et al. (1998)	5.6
J0552+0313	0552+032	05 52 50.101502	03 13 27.24314	1.01	Beasley et al. (2002)	4.2

extended atmosphere with the VLA in A configuration and the VLBA Pie Town antenna to obtain maximum spatial resolution. As part of this radio study we have also obtained new multi-epoch radio positions.

In this paper we combine radio positions from our observing programs and archival data, published VLA positions, and the *Hipparcos* Intermediate Astrometric Data (IAD) to obtain new astrometric solutions and parallaxes for Betelgeuse. In Section 2 we present our new radio positions together with previous measurements, and in Section 3 we discuss the Hipparcos IAD for Betelgeuse. In Section 4 we combine all these datasets to find an improved astrometric solution, and in Section 5 we discuss the implications of the new astrometric solutions for Betelgeuse, including its stellar parameters, the wind–interstellar medium (ISM) bow shock identified in IRAS images by Noriega-Crespo et al. (1997), and the likely birthplace of Betelgeuse. Conclusions are given in Section 6.

2. VLA STELLAR POSITION MEASUREMENTS

The large cosmic error/noise term in the *Hipparcos* solution may be of stellar origin, perhaps related to movements of the photocenter, of order 3.4 mas, in the *Hipparcos* photometric H_p band (Bessell 2000). In M supergiants this passband and also the V band contain TiO opacity which is sensitive to changes in surface temperature. One can imagine that above the photospheric granulation pattern there are regions of different temperature with differing contributions to the flux in the H_p band. The convective turn-over timescale is ∼150–350 days (see Josselin & Plez 2007); however, most of the *Hipparcos* measurements occur over two intervals each spanning <92 days, so photocenter jitter is an unlikely explanation for the source of cosmic error.

The thermal continuum emission at radio wavelengths provides a different view of the star, covering the outer photosphere, chromosphere, and the base of the stellar wind (Harper et al. 2001). The collisional source function is the Planck function on the Rayleigh–Jeans tail, which is linear in electron temperature, and the specific intensity is therefore less sensitive to surface temperature inhomogeneities on the stellar disk than the Planck function at optical wavelengths at $T_{\rm eff} \sim 3600$ K. The VLA therefore provides new 2D position measurements which possess different kinds of systematic uncertainties, such as non-random extended structures related to non-radiative heating and mass loss. However, centimeter continuum radio opacity is a well-defined function of frequency and temperature, so that by considering multiwavelength positions obtained at the same epoch we can examine and quantify these potential systematic uncertainties.

2.1. New Multiwavelength VLA Observations

We have obtained a sequence of high spatial resolution VLA observations of Betelgeuse in 2002–4 (programs AH0778 & AH0824) to study the temporal evolution of Betelgeuse's resolved atmosphere and to constrain thermodynamic changes that occur when mechanical energy is deposited to form the chromosphere and to drive the stellar outflow. The hot chromosphere is visible in the ultraviolet and confined to a small volume filling factor (Harper & Brown 2006), while the bulk of the extended atmosphere is cool (Lim et al. 1998).

We have used the highest spatial resolutions available with the VLA, i.e., A-configuration with the Pie Town VLBA antenna, and these allow us to obtain positional uncertainties comparable to *Hipparcos*. Good u–v coverage was obtained for six frequency bands (Q, K, U, X, C, L)[7] at five epochs. For each band we used two 50 MHz continuum channels recording full Stokes polarizations. The analysis of these datasets provides source size and intensity as functions of wavelength and epoch. In this paper we present the positions of Betelgeuse, while the thermodynamic study will be presented in a later publication.

The VLA observations were made by repeatedly interleaving observations of Betelgeuse, which is slightly offset from the field center by a couple of synthesized beam widths in order to avoid potential errors at phase center, with a primary phase calibrator over a long enough range of time to ensure good u–v coverage. Typically, each 11.5 h observation provided ∼7 h of on-source data for α Ori. Our observing sequence cycled through the full set of frequency bands roughly every 2 h. The primary phase calibrator (J0532+0732, see Table 4 for calibrator details) has an accurate position in the ICRF (Ma et al. 1998), and the phase solutions from this calibrator are used to correct for temporal tropospheric phase fluctuations which are then transferred to the Betelgeuse field. J0532+0732 is separated by 5.6° from Betelgeuse and provides accurate positions of Betelgeuse in the ICRF. The phase calibrator (J0552+0313), which is fainter and separated by 4.2° from Betelgeuse, was used by Lim et al. (1998). Atmospheric phase errors are proportional to frequency so that at shorter wavelengths a more rapid cycle between the source and the phase calibrator, which established the source position, is required. At the three shortest wavelength bands (Q, K, and U) an efficient source–phase calibrator fast-switching technique was employed (Carilli & Holdaway 1997). These three bands were observed only at elevations greater than ∼20°. Source–phase calibrator fast-switching cycle times of 2–3 min were used depending on the weather conditions. Reference pointing on the phase calibrator at X band was performed prior to each section of fast switching. At the longer wavelengths a conventional calibrator–object–calibrator sequence was used with the Betelgeuse observations lasting between 8 and 12 min. Each 11.5 h observation provided on-source data for Betelgeuse of roughly 0.5 h at Q, 1.0 h at K and U, and 1.5 h at X, C, and L bands. The Q band was not observed in our 2002 datasets.

The data were calibrated and edited within the Astronomical Image Processing System (AIPS). Time intervals with instrumental problems or poor phase stability were identified using the tasks TVFLG and CALIB and flagged. The calibrated data

[7] These bands have nominal wavelengths: $Q = 0.7$ cm, $K = 1.3$ cm, $U = 2.0$ cm, $X = 3.6$ cm, $C = 6$ cm, and $L = 20$ cm.

Table 5
J2000 Radio Positions of Betelgeuse

Epoch Julian Year	R.A. (J2000)	Error (mas)	Decl. (J2000)	Error (mas)	Reference
2004.829	05 55 10.31227	2.5	07 24 25.4615	3.3	AH0824: Q, K, U, X, C, L
2004.805	05 55 10.31225	2.0	07 24 25.4616	4.8	AH0824: Q, K, U, X, C, L
2003.609	05 55 10.31045	4.1	07 24 25.4574	2.4	AH0824: Q, K, U, X, C, L
2003.4356	05 55 10.3097	5	07 24 25.461	12	AF0399: X, Boboltz et al. (2007)
2002.280	05 55 10.30752	1.8	07 24 25.4383	4.9	AH0778: K, U, X, C, L
2002.132	05 55 10.30725	1.7	07 24 25.4362	3.1	AH0778: K, U, X, C, L
2000.991	05 55 10.30519	1.2	07 24 25.4193	1.3	AL0525: Q, K
2000.943	05 55 10.3061	13	07 24 25.432	26	AF0376: X, Boboltz et al. (2003)
1998.241	05 55 10.30147	3.1	07 24 25.4014	5.7	AL0436: Q, K
1996.971	05 55 10.29911	8.9	07 24 25.3983	5.9	AL0398: Q, K, U, X
1987.655	05 55 10.28378	15	07 24 25.2867	15	AB0446: U
1982.4261	05 55 10.27623	30	07 24 25.2663	30	C, Johnston et al. (2003)
1982.4181	05 55 10.27564	30	07 24 25.2293	30	C, Johnston et al. (2003)

Notes.
The VLA program numbers are given for the new positions. The R.A. and decl. include guard figures. These positions were used to derive astrometric solution No. 4, while solution 3 includes our *X*-band data and thus the relevant epochs have slightly different positions and errors.

were CLEANed and imaged using IMAGR for comparison to our u–v plane fitting results.

Positions of extended sources are frequently measured from radio maps using a simple function for the source specific intensity such as a 2D Gaussian or a 2D uniform ellipse. Since Betelgeuse is neither a Gaussian nor a uniform ellipse, we have created a custom 2D specific intensity profile that is a function of wavelength. This intensity function is derived from the semi-empirical 1D spatially-resolved thermodynamic model of Harper et al. (2001). The relationships between the radio opacity and source function at adjacent wavelengths are accurately known, so that multiwavelength observations allow the temperature and mean density distributions, and hence the wavelength-dependent specific intensity distributions, to be very well constrained. The specific intensity distributions are shown in Brown & Harper (2004), and have been generalized to have a 2D elliptical form for greater flexibility.

This empirical multiwavelength approach to derive the spatial specific intensity profiles is necessary because the source is resolved and there are no theoretical models for the brightness distributions resulting from the processes that extend the atmospheres and drive mass loss from evolved cool stars like Betelgeuse. These phenomena are the result of energy and momentum being deposited into the atmosphere so that the energy balance and thermal structure are not known *a priori*. Note that in the absence of sufficient observational constraints additional assumptions must be made, e.g., a prescribed temperature structure for Mira stars (Reid & Menten 1997).

The 2D intensity model fits are made on both the individual visibilities and on a grid of binned data with different u–v cell sizes which allows the goodness of fit to be established. The formal error of the 2D fits for individual wavebands are smaller than the difference in position between the bands. We also find that the positions measured with different u–v bin sizes are very similar, and that the positions measured in the image map with JMFIT are very close to those measured in the visibility data. Boboltz et al. (2003) find that their formal fitting errors are typically smaller than the scatter of individual position measurements made at a given frequency. These trends suggest that some residual phase errors remain.

2.2. Published VLA Positions

Radio positions of Betelgeuse have been published by Johnston et al. (2003), Boboltz et al. (2003), and Boboltz et al. (2007). The two 1982 positions were obtained at *C* band (6 cm) with a single 50 MHz channel (Johnston et al. 2003), while the 2000 and 2003 Boboltz et al. observations were made with two 50 MHz channels at *X* band (3.6 cm) in A configuration with the Pie Town antenna. Boboltz et al. (2003, 2007) have taken advantage of the long time interval (21 yr) to derive a proper motion (see Table 3). Their $\mu_{\alpha\cos\delta}$ and μ_δ are about 1.5σ and 0.5σ below the nominal *Hipparcos* values, respectively. The accuracy of these VLA positions is sufficient to constrain the proper motions, but not the parallax directly.

2.3. Archival Observations

To increase the number of epochs with radio positions we calibrated and measured several less comprehensive datasets from the NRAO archive, including the data described by Lim et al. (1998). The program numbers are given in Table 5. The high frequency observations of Lim and colleagues (programs: AL) also used the fast-switching technique.

2.4. VLA Positions

For each epoch where we have more than one wavelength observation, we use the formal errors of the centroid position fits for each band to form a weighted mean position. The size of these errors reflects the quality of the phases, the u–v coverage, and deviations in source intensity from that which is symmetric by a rotation of 180°. We estimate the uncertainty in the epoch positions by taking the standard deviation of the positions measured in each band about the weighted mean position and adding in quadrature the mean formal fitting error and phase calibrator uncertainty. For the 1987 single-frequency *U*-band position we assign an uncertainty of 15 mas. In Table 5 we give the measured positions of Betelgeuse and their 1σ uncertainties. The Julian date is given for the mid-time of the observing session, or that from the published sources. The positions we have measured have been corrected to the phase calibrator positions given in Table 4, especially for J0552+0313

because the position given for this calibrator in the VLA Calibrator List has changed significantly over time. This results in the phase center used for the calibrator being slightly offset from its true position and this then introduces a corresponding positional offset in the calibrated Betelgeuse data.

One potential source of variation of apparent stellar position with wavelength is the presence of large-scale structures in the stellar atmosphere. In that case the positions at adjacent wavelengths should vary smoothly because the flux contribution functions have significant physical (spatial) overlap. To investigate the potential magnitude of this effect we have examined the 3D radiative hydrodynamic simulations of Betelgeuse by B. Freytag and collaborators (Freytag et al. 2002; Chiavassa et al. 2006). While there are no models that describe the thermal structure of the extended M supergiant atmospheres, the Freytag models describe the convective structure of the underlying photosphere. We find that the photocenter changes with viewing angle at the fraction of a milliarcsecond level, while the change with VLA frequency in a given snapshot is smaller. The temperature contrast between the real hot chromosphere and cool wind is larger than in the photosphere and therefore radio photocenter changes of order 1 milliarcsec would not be unexpected. It is possible that some of the subtle *Q*–*K*–*U* position drifts seen in the 2004 data may be stellar in origin.

Many of the more recent datasets have good *u*–*v* coverage and long observation times and the source is sufficiently resolved that the formal fitting errors of the intensity centroid are <1 mas and the positional uncertainties are ∼3 mas and thus comparable to those obtained for point sources with the VLBA. For the highest S/N data one is struck by the high repeatability of the radio positions, for example the 2000.991 datum is a mean of *Q*- and *K*-band observations taken a week apart, yet their individual positions are within a fraction of a milliarcsecond in both R.A. and decl. While the precision of many of the observations is very high our results are likely dominated by systematic uncertainties with respect to the position of the center of mass of the star. Our two 2004 datasets were obtained a week apart and these have small formal errors. In R.A. both datasets show a small decline in position with increased wavelength: *Q*–*K*–*U*–*X* with a 9 mas range, while in declination a similar decline is seen in *Q*–*K*–*U* but the *X* band increases by 10 mas. We find a similar jump in declination in all our *X*-band data, but not the Lim et al. (1998) 1996 data. Another advantage of the multiwavelength datasets is that the atmospheric phase errors are proportional to frequency, so that different wavelengths should be affected systematically to different degrees. The *X*-band data were not obtained with fast switching and we may be detecting signs of systematic error in the *X*-band radio positions. The ionosphere can affect *X*-band positions and more so *C*-band. We therefore compared our *C*-band positions and found that they clustered nearer to the *Q*-, *K*-, and *U*-band positions rather than following the trend observed in the *X* band. We can offer no explanation for the behavior of our *X*-band data, so in Section 4 we consider the effect of including and excluding our *X*-band data on the new astrometric solutions.

3. *HIPPARCOS* ASTROMETRIC SOLUTION

We have derived new astrometric solutions for Betelgeuse by combining the VLA radio positions with the *Hipparcos* IAD, which are described below. The IAD are given with respect to the *Hipparcos* astrometric solution (ESA 1997) (given in Table 2) and we used the *Hipparcos* solution as the reference solution in the following.

3.1. Intermediate Astrometric Data

The IAD are described in detail by van Leeuwen & Evans (1998). The *Hipparcos* Catalogue (ESA 1997) represents the merged results of two independent data reduction consortia, NDAC (Lindegren et al. 1992) and FAST (Kovalevsky et al. 1992). For Betelgeuse, there were 18 NDAC and 20 FAST great circle reductions and the results were merged to obtain the final astrometric solution. The abscissa residuals Δv, the 1D offset from the final solution that is shown in Table 2, are given in the IAD provided by the two consortia in the catalog, along with the partial derivatives that define

$$\Delta v = \sum \frac{dv}{da} \Delta a$$

where $\Delta a = a_{\rm new} - a_{\rm Hipparcos}$. The *Hipparcos* astrometric solution is that which minimizes the square of the residuals.

The NDAC and FAST abscissa residuals for a given great circle are correlated and the correlation coefficient is also provided in the IAD. The IAD provides all the information needed to decorrelate and properly weight the pair of great circle solutions (van Leeuwen & Evans 1998). The resulting equations can then be combined with other measurements, such as the 2D radio positions, in a least-squares solution to improve the overall astrometric solution, which we do in Section 4.

As discussed in Section 1, Betelgeuse required a significant additional error source (*cosmic noise*) to obtained the expected χ^2. The actual nature of this cosmic noise is not known but it may be related to photocenter movement which is unlikely to be random in position on short timescales and would likely provide a systematic error in the astrometric solution. The position angle of the star's rotation axis has been measured from spatially resolved ultraviolet *Hubble Space Telescope* spectra. Uitenbroek et al. (1998) found ∼55° (measured East of North) from absorption features in Goddard High Resolution Spectrograph data, and Harper & Brown (2006) found ∼65° from emission features in multi-epoch Space Telescope Imaging Spectrograph data. The distribution of photocenters, perhaps driven by convective and Coriolis terms, may have a special relation to the rotation axis. The stellar proper motion vector also has a position angle of 68° and brightness fluctuations that occurred preferentially near the stellar equator might induce scatter in the parallax displacements, although fluctuations due to stellar rotation itself, would be unlikely because of the ∼17 yr rotational period (Uitenbroek et al. 1998).

The position of the stellar image on the *Hipparcos* detector is a function of effective wavelength that has been calibrated in the Catalogue using non-contemporaneous Cousins $V - I$ colors. A constant $V - I = 2.32$ was used for Betelgeuse in the *Hipparcos* solution. Changes in the actual stellar $V - I$ during the *Hipparcos* mission could, therefore, lead to movement of the apparent stellar positions induced by color variability. This was seen in Mira stars whose colors change significantly on timescales near 1 yr (Pourbaix et al. 2003). Betelgeuse shows irregular photospheric variations on 5.78 yr (Sanford 1933) and 420 day (Dupree et al. 1987; Smith et al. 1989) timescales. The shorter of these periods may potentially cause some color induced movement in the apparent stellar position, or an offset caused by differences in adopted and actual mean $V - I$ color may lead to a slight systematic error. Platais

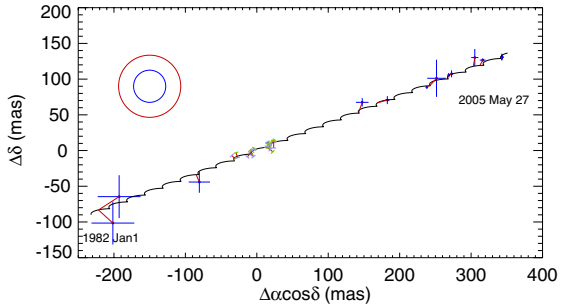

Figure 1. The predicted and observed positions of Betelgeuse. The positional data considered in this paper are shown with the predicted positions of Betelgeuse (black curve) based on astrometric solution No. 4. The begin and end dates of the black curve are given. The circles show typical angular diameters of the source: blue (optical: 45 mas) and red (radio 7 mm: 87 mas). The red lines link the measured positions (blue) to the predicted positions. 1σ errors are shown. The *Hipparcos* data are shown in more detail in Figure 2.

et al. (2003) derived relationships between contemporaneous *Hipparcos/Tycho* photometry and Cousins $V - I$ colors that allow one to derive approximate corrections to the abscissa residuals based on photometry obtained at the same epoch. We combined the H_p and V_T epoch photometry from the *Hipparcos* Photometry Annexes with NDAC calibration data (kindly provided by L. Lindegren) to estimate changes in the abscissa residuals for both consortia following Pourbaix et al. (2003). The astrometric solution was little affected, with the cosmic noise dominating the small changes in abscissa residuals, and we conclude that color induced abscissa errors are not the cause of the cosmic noise.

4. REVISED VLA & *HIPPARCOS* ASTROMETRIC SOLUTION

We now combine the 2D radio positions (α,δ) with the 1D *Hipparcos* IAD to derive new five-parameter astrometric solutions for Betelgeuse. The square of the residuals for twice the number of radio positions + 38 IAD decorrelated equations were minimized. The *Hipparcos* cosmic error value was retained for the IAD, although the expected change in proper motion would actually lead to a slight increase in its value. The JPL planetary ephemeris was used to calculate the apparent stellar position for a given set of five astrometric parameters. Using the IAD data and the cosmic error, the *Hipparcos* solution and covariance matrix were reproduced.

The earlier radio positions of Boboltz et al. (2003) and Johnston et al. (2003) have larger uncertainties than the IAD abscissa residuals and cosmic noise, but they do cover a long time span (21 yr) and clearly demonstrate the need for a downward revision in both components of the proper motion. They do not, however, constrain the parallax. Our multiwavelength radio positions have smaller uncertainties (from the weighted multiwavelength positions) and these provide significant new constraints on the parallax and proper motion.

In Table 6 we provide the astrometric solutions based on different criteria and data sets. The first two use the *Hipparcos* data with fixed proper motions. The solutions are: (1) IAD with fixed FK5 proper motions; (2) IAD with the proper motion given by Boboltz et al. (2007); (3) all VLA positions and IAD, and (4) VLA positions (excluding our X-band data) and IAD. The 1σ errors of the new astrometric solutions have been scaled (increased) to obtain a reduced $\chi^2 = 1$. The goodness-of-fit measure shows that systematic errors are present in the radio

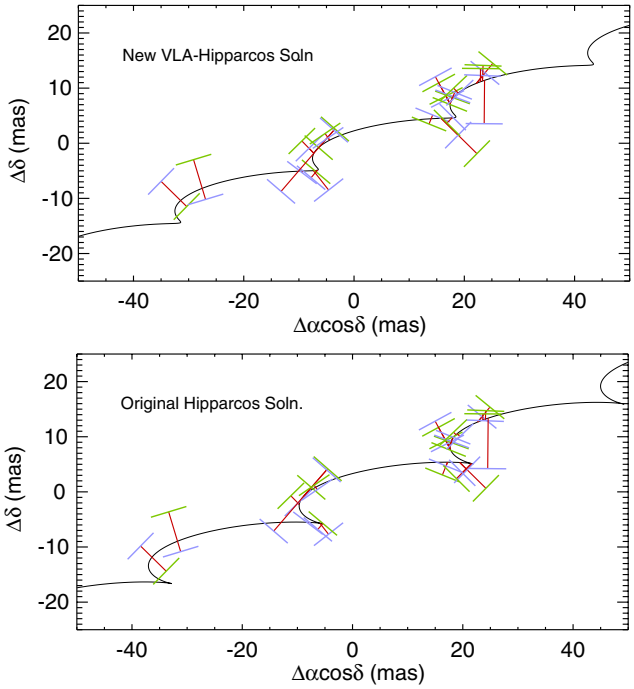

Figure 2. Top: Enlargement of the new astrometric solution showing the *Hipparcos* IAD. These are a 2D representation of the 1D abscissa data from the FAST (green bar) and NDAC (blue bar) consortia. The measured source position is offset from the astrometric solution by the length of the red connecting line, but its position along the bar is unknown. For most great circle solutions there are matching FAST and NDAC solutions. The total length of the green and blue bars is arbitrarily shown with 2× the additional cosmic error/noise given in the *Hipparcos* solution (i.e., 2 × 3.36 mas). The instrumental abscissa error is only ∼2.2 mas. Bottom: The original *Hipparcos* solution is shown for comparison.

data; however, we have not added any *cosmic radio noise* to the radio positional uncertainties as was done in the *Hipparcos* solutions.

Figure 1 shows all the data included in astrometric solution No. 4 and emphasizes the 24 yr span of the datasets. Figure 2 (top) shows an enlargement of the solution and shows how the IAD fit the new combined solution, and (bottom) the original *Hipparcos* solution. Figure 3 shows enlargement of the recent VLA radio positions.

Fixing the proper motions in solutions (1) and (2) does not change the parallax significantly. However, when the radio positions are included the parallax decreases. Because the IAD data favors a larger parallax the *Hipparcos* and VLA datasets are in tension. As noted in Section 2.4, there is an indication that X-band is systematically offset in declination in our data from the Q-, K-, and U-band positions, so in solution No. 4 we further exclude our X-band positions from the weighted epoch positions. In this solution the positions errors on decl. and this is our preferred solution.

Solution No. 4 provides a distance of 197 ± 45 pc to Betelgeuse, which is greater than the original *Hipparcos* values of 131 ± 30 pc. The inclusion of the radio positions into the combined astrometric solution has reduced both proper motions, as found previously from VLA only data by Boboltz et al. (2007). The parallax, however, is reduced by ∼2σ from the original *Hipparcos* value leading to a greater stellar distance, size, luminosity, and space motion. The combined solution for the parallax is in a sense a mean of the original *Hipparcos* value and that from the radio data alone. The radio data are not currently sufficient to define a reliable parallax, but they

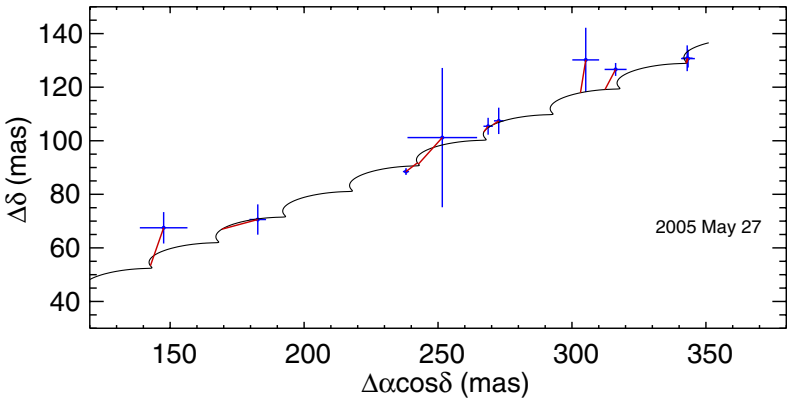

Figure 3. Enlargement of the post-*Hipparcos* VLA radio positions which exclude our *X*-band data. The small errors on the VLA positions provides sufficient weight in the combined solutions to reduce the parallax from its original *Hipparcos* value. The two largest error bars are the single frequency *X*-band Boboltz et al. positions. The epoch 2000.991 position has a very small estimated uncertainty and provides tension in the proper motions with the 2002 and 2004 positions. Increasing the uncertainty of the 2000.991 position to that of the smallest of our uncertainties leads to an increase in distance to 220 pc, i.e., 0.5σ.

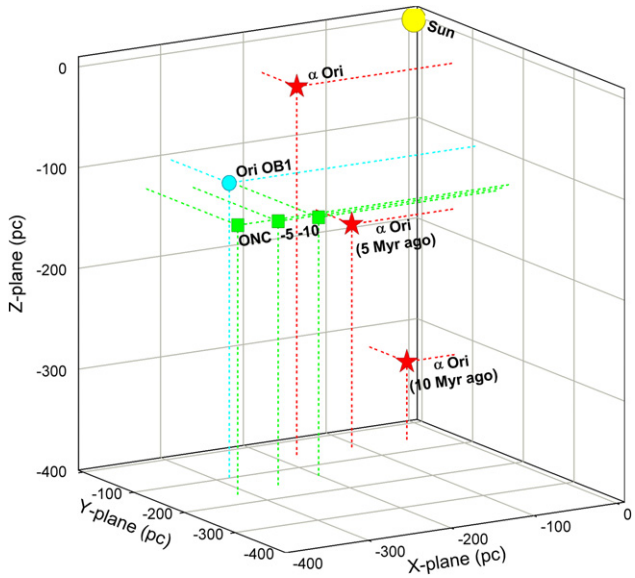

Figure 4. Schematic representation of Betelgeuse's position as a function of age in galactic coordinates, compared to the positions of the young Orion Nebula Cluster (ONC) and the older Ori OB1 association. The motion of Betelgeuse is very different from the ONC which has a small velocity in the *Z*-direction (W′). The most likely formation scenario for Betelgeuse is as a runaway star from the extended Ori OB1 association which has a similar age. Betelgeuse's W′ then would likely be the result of expulsion from a high mass multiple system.

suggest a value ∼330 pc (with a large uncertainty). New multiwavelength radio observations are needed to improve the parallax.

4.1. Comparison with the New Hipparcos Reduction

A new reduction of the *Hipparcos* raw data has very recently become available (van Leeuwen 2007). One feature of this reduction is significantly smaller astrometric formal errors for bright stars. The new *Hipparcos* solution for Betelgeuse is given in Table 7 and compared with the original and our No. 4 solution. It can be seen that the formal errors for proper motions are decreased by more than a factor of 2. Both the revised $\mu_{\alpha\cos\delta}$ and μ_δ are $>2\sigma$ different from our new combined result. The revised *Hipparcos* parallax leads to a larger distance (152 ± 20 pc) than the original; however, the astrometric solution still requires a significant *cosmic noise* of 2.4 mas. Given these results it is clear that the *Hipparcos* data still contain systematic errors of unknown origin.

The radio data also suffer from unknown systematic errors and it is our hope that by combining these two datasets the new solution mitigates the effect of these errors on the solution.

5. DISCUSSION

Now we discuss some of the implications of different distance estimates for Betelgeuse's interaction with its local environment, stellar parameters, and its place of birth. In the following we adopt our new nominal distance of 200 pc.

5.1. Betelgeuse's Wind-ISM Bow Shock

As Betelgeuse travels through its local interstellar environment, its massive M supergiant wind plows up material forming an asymmetric arc observable in high-resolution *IRAS* 60 μm and 100 μm images (Noriega-Crespo et al. 1997). The apex of the arc has a position angle of $60^\circ \pm 10^\circ$, a mean thickness of 1.5 arcmin, and an inner radius of 5 arcmin from the star (Noriega-Crespo et al. 1997) which at 200 pc corresponds to a mean physical projected radius of 0.33 pc. Within 2′ NE of the arc there is a straight bar that may be cirrus, i.e., interstellar dust heated by the ambient radiation field.

The radial velocity of Betelgeuse is best determined from photospheric radial velocity observations when the 5.78 yr pulsation signature is most stable, i.e., when the radial velocities are least stochastic (Goldberg 1984). In Table 1 we give the mean of the Jones (1928) and Sanford (1933) values, i.e., $V_{\rm rad} = +20.7 \pm 0.4$ km s^{-1} (heliocentric) moving away from the Sun. The tangential velocities (in km s^{-1}) at a distance D are $V_{\alpha\cos\delta} = 23.7[D(pc)/200]$ and $V_\delta = 9.1[D(pc)/200]$, with a position angle of 69.0° east of north, which is consistent with the infrared arc's orientation. The new astrometric solution corresponds to a galactic space velocity of $U = -21.7, V = -11.5, W = +21.2$ km s^{-1}, where U is positive towards the Galactic center. Correcting for the solar motion, the space motion in the local standard of rest (LSR) is $U' = -12.7, V' = +0.5, W' = +28.2$ km s^{-1}.

If the arc is a result of a wind bow shock, the standoff distance ($R_{\rm so}$) is where the ram pressure of the wind balances that of the

Table 6
New Astrometric Solutions for Betelgeuse

Solution	$\Delta\alpha\cos\delta$ (mas)	Error (mas)	$\Delta\delta$ (mas)	Error (mas)	π (mas)	Error (mas)	$\mu_{\alpha\cos\delta}$ (mas yr^{-1})	Error (mas yr^{-1})	μ_δ (mas yr^{-1})	Error (mas yr^{-1})
(0) Hipparcos	0.00	1.51	0.00	1.13	7.63	1.64	27.33	2.30	10.86	1.46
(1) Hipp + FK5 μ's	0.51	1.38	0.85	0.91	7.11	1.51	25.0	...	9.0	...
(2) Hipp + VLA μ's	0.52	1.39	0.55	0.91	7.32	1.51	23.98	...	10.07	...
(3) Hipp + All VLA (Q, K, U, X)	−0.20	1.77	0.85	1.20	4.32	1.29	24.93	0.10	9.42	0.18
(5) Hipp + VLA (Q, K, U, X†)	−0.06	1.80	0.60	1.21	5.07	1.10	24.95	0.08	9.56	0.15

Notes.
ICRF Epoch 1991.25. R.A. and decl. are given with respect to the *Hipparcos* Solution (given in Table 1). X† denotes that we have excluded our *X*-band data.

Table 7
Comparison of New and Original Hipparcos Results with the New *Hipparcos* Reduction

Parameter	Value (mas yr^{-1} or mas)	Uncertainty (mas yr^{-1} or mas)	Source
$\mu_{\alpha\cos\delta}$	27.33	2.30	Old *Hipparcos*; ESA (1997)
$\mu_{\alpha\cos\delta}$	27.54	1.03	New *Hipparcos*; van Leeuwen (2007)
$\mu_{\alpha\cos\delta}$	24.95	0.08	This work
μ_δ	10.86	1.46	Old *Hipparcos*; ESA (1997)
μ_δ	11.32	0.65	New *Hipparcos*; van Leeuwen (2007)
μ_δ	9.56	0.15	This work
π	7.63	1.64	Old *Hipparcos*; ESA (1997)
π	6.56	0.83	New *Hipparcos*; van Leeuwen (2007)
π	5.07	1.10	This work

surrounding material, i.e.,

$$R_{\rm so} = \sqrt{\frac{\dot{M} V_\infty}{4\pi\rho V_*^2}} \quad (1)$$

(Wilkin 1996), where V_* is the peculiar motion of the star with respect to the local medium of density ρ, and V_∞ and $\dot{M}$ are the wind outflow speed (in the frame of the star) and mass-loss rate, respectively, at the distance $R_{\rm so}$ from the star. Circumstellar absorption features indicate $V_\infty \simeq 17$ km s^{-1} (Bernat et al. 1979), and a representative estimate of the mass-loss rate is $\dot{M} \simeq 3\times10^{-6}\ M_\odot$ yr^{-1} (Harper et al. 2001). Betelgeuse has a small radial velocity in the LSR, and the Sun's peculiar motion is directed away from Betelgeuse contributing most of the observed heliocentric radial velocity. If the environs near Betelgeuse are at rest in the LSR, we can estimate the star's peculiar velocity with respect to the LSR as $V_* \simeq \sqrt{V_{\alpha\cos\delta}^2 + V_\delta^2} \simeq 25$ km s^{-1} and the bow shock will be viewed close to edge on. These values then provide an estimate of the density of the material surrounding the star.

When the stellar motion in and out of the plane of the sky is small, the hydrogen density of the material being swept-up by the stellar wind (n_H) is given by

$$\frac{n_H}{\rm cm^{-3}} \simeq \frac{3.7\times10^7}{\Sigma}\left(\frac{D}{\rm pc}\right)^{-2}\left(\frac{\theta}{\rm arcmin}\right)^{-2}\left(\frac{\dot{M}}{10^{-6}\ M_\odot\ {\rm yr}^{-1}}\right) \times\left(\frac{V_\infty}{\rm km\ s^{-1}}\right)\left(\frac{V_*}{\rm km\ s^{-1}}\right)^{-2} \quad (2)$$

where Σ is the mean mass per hydrogen nucleus (∼1.4) of the surrounding material, and θ is the observed angle between the star and the bow shock. Since $V_* \propto D$, then n_H is a strong function of distance, $n_H \propto D^{-4}$.

The initial analysis of the enhanced resolution *IRAS* images by Noriega-Crespo et al. (1997) assumed a stellar distance of $D = 400$ pc and adopted a mean shell distance of $\theta \sim 7$ arcmin, and obtained $n_H \simeq 0.1$ cm^{-3} which is typical of the local ISM. (This should have been $n_H \simeq 0.05$ cm^{-3} because the power of the mean mass has an incorrect sign in Equations (1) of van Buren & McCray 1988 and Noriega-Crespo et al. 1997)

The original and revised *Hipparcos* distances of 131 pc and 152 pc, respectively imply a major change in the inferred hydrogen density. The large reduction in distance by a factor of ∼3 leads to a large increase to $n_H \simeq 2-3$ cm^{-3}, which is inconsistent with the picture of the local ISM towards galactic coordinates $l = 200°$, $b = -9°$, namely, a hydrogen column density of $N_H \leqslant 10^{19}$ cm^{-2} with $\bar{n}_H \leqslant 0.05$ cm^{-3} (Paresce 1984), and $\bar{n}_H \simeq 0.3$ cm^{-3} for material in front of the Orion OB association (Frisch et al. 1990).

The wind-ISM bow shock model with our new VLA-*Hipparcos* distance implies a smaller but still high local density of $n_H \sim 1$ cm^{-3}. For distances greater than 75 pc, beyond the Local Bubble (Lallement et al. 2003), Betelgeuse lies near the edge of a cavity of low neutral hydrogen density and close to a steep gradient in ISM column density between $l = 180°$–$200°$. It is possible that the increase in ISM column density in this region is associated with larger particle densities. Visual inspection of the *IRAS* images reveals an interesting detail: the shape of the 60 μm and 100 μm arcs are rather circular. However, the ratio of the angular separation of the arc apex and the arc at 90° to the apex in this idealized wind-ISM bow shock model should be close to $1/\sqrt{3}$ (Wilkin 1996), which is smaller than observed and the discrepancy gets worse if there is a radial velocity component with respect to the LSR. This may mean that the arcs are shaped by an interaction of stellar mass loss at past and present epochs rather than direct interaction with the interstellar medium.

Table 8
Stellar Properties Inferred as a Function of Distance

Property	Distance		
	150 pc	200 pc	250 pc
Bolometric luminosity (ergs s^{-1})	4.87	5.12	5.31
Initial mass ($M_\odot$)	~17	~20	~24
Age (10^6 Yr)	~13	~10	~8
Space velocity (LSR)[U', V', W'] (km s^{-1})	[−12, 2, 22]	[−13, 0, 29]	[−13, −1, 35]

Note. For the space motions the proper motions are held constant.

In the bow shock scenario, the flow velocities are low enough that the post-shock cooling length is smaller than the shell thickness and the wind-ISM shock is potentially unstable. The isothermal stellar wind bow shock instabilities examined by Blondin & Koerwer (1998) have length scales of the order of the standoff distance, which is larger than suggested by the *IRAS* images. The ratio of Betelgeuse's peculiar velocity to the wind speed is only $V_*/V_\infty \simeq 1.5$ and as a consequence it might only be modestly unstable (Dgani et al. 1996). New AKARI, and future higher spatial resolution and more sensitive far-infrared images, may help clarify the nature of the infrared arcs and any substructure they contain.

5.2. Stellar Properties

α Sco (M1 Iab + B3 V: Antares) and CE Tau (M2 Iab-Ib: 119 Tau) are both nearby M supergiants with spectral types close to that of Betelgeuse (M1-M2 Ia-Iab). The MK designations are from Keenan & McNeil (1989), and change by a sub-type during the erratic pulsation cycle. Betelgeuse might be slightly more luminous than α Sco which has a similar angular diameter and pulsation period. α Sco also has a large uncertainty in its *Hipparcos* parallax, 5.40 ± 1.68 mas, and it also has essentially the same cosmic error 3.37 ± 0.59 mas. CE Tau is more distant ($\pi = 1.70 \pm 0.80$ mas), and although it has a smaller parallax uncertainty its distance is also uncertain. The paucity of local M supergiants makes it difficult to calibrate observational diagnostics that might provide additional constraints on the stellar distances.

Different estimates of Betelgeuse's observed (de-reddened) integrated bolometric flux are in reasonable agreement, in part because of the low interstellar and circumstellar extinction near the stellar flux peak: i.e., $F_{\rm Bol} = 1.0 \pm 0.1 \times 10^{-4}$ erg cm^{-2} s^{-1} (Harper et al. 2001), and $F_{\rm Bol} = 1.1 \pm 0.1 \times 10^{-4}$ erg cm^{-2} s^{-1} (Perrin et al. 2004), and the luminosity is then given directly in terms of distance by

$$\log \frac{L}{L_\odot} = 5.12 + 2 \log \left(\frac{D}{200 pc} \right).$$

At a distance of 197 pc with the uncertainty from our parallax measurement Betelgeuse would have a bolometric luminosity of $\log L/L_\odot \simeq 5.10 \pm 0.22$ (1σ). This corresponds closely to the 20 $M_\odot$ stellar evolution model of Meynet & Maeder (2003) which would have a main-sequence spectral-type of O9 V. This set of models, which includes the effects of mass loss and rotation, are probably the most appropriate set for comparison to Betelgeuse (see Levesque et al. 2005). Table 8 shows the implied properties of Betelgeuse for different assumed distances. The radius of Betelgeuse is then 950 $R_\odot$ both from the observed near infrared photospheric angular diameter ($\phi = 45$ mas, e.g. Perrin et al. 2004) and from the measured luminosity and an effective temperature of 3650 K (Levesque et al. 2005). The evolutionary models suggest that the current mass of the star is 18 $M_\odot$ which corresponds to a surface gravity of 0.5 cm s^{-1}. At the 2σ upper bound to the distance of 300 pc the bolometric luminosity is $\log L_{\rm bol} = 5.47$, which is close to the 25 $M_\odot$ model of Meynet & Maeder (2003).

Indirect estimates of the luminosity can be made using period–luminosity relations. Turner et al. (2006) presented an empirical period–luminosity relation for semi-regular (SRc) M supergiant variables in Per OB1 and Berkeley 87, and found that the relation was consistent with selected linear non-adiabatic pulsation models of Guo & Yi (2002). Betelgeuse shows at least two periods and both the 5.78 yr and 400 day periods are observed in radial velocity and light curves, although the radial velocities and light curves are not tightly correlated. The Turner et al. (2006) relation for Betelgeuse's shorter period, similar to BU Per, T Per, and SU Per (Kiss et al. 2006; Stothers 1969) implies $\log L/L_\odot \simeq 4.75$, which is consistent with the *Hipparcos* distance, while the Kiss et al. (2006) period–K-magnitude relation gives 200 ± 40 pc which is close to our preferred distance.

Betelgeuse's radial velocity amplitude, when present, is similar for both periods so that the longest period leads to the largest change in radius and may be the fundamental mode. Wasatonic et al. (2005) also found dual photometric periods of 350–450 days and 6.16 yr for TV Gem (M1 Iab) and concluded that the 6.16 yr period was the fundamental mode. Only the models more massive than 18 $M_\odot$ in Guo & Yi (2002) have fundamental and first overtone periods that have these range of values and luminosities consistent with our revised distance. However, from their analysis of brightness variations in M supergiants, Kiss et al. (2006) conclude that the long secondary periods (i.e., >1000 days) are not radial pulsations in accord with Stothers & Leung (1971). Clearly period–luminosity relations, observational or theoretical, are not yet sufficiently well understood to help constrain Betelgeuse's distance, and we note that the large fractional radius changes associated with the longer periods have yet to be fully addressed by theoretical pulsation models.

Some previous estimates of the distance have used the V magnitude. We do not anticipate significant interstellar reddening in Betelgeuse's line-of-sight, but there will be some visual extinction associated with the circumstellar dust shell. Betelgeuse is oxygen rich, and its dust shell has been modeled with silicate grains, e.g., Rowan-Robinson et al. (1986). Silicates grains with characteristic radius 0.1 μm have a high albedo in the V band and in the ultraviolet between 2000–3000 Å. We can estimate the visual dust absorption by noting that low intrinsic optical depth ultraviolet emission lines observed in *International Ultraviolet Explorer* (*IUE*) spectra are *not* systematically redshifted with respect to the star (Carpenter 1984). The emission

line Doppler line widths are comparable to the gas wind speed (i.e., 17 km s^{-1}), and the $R \sim 12{,}000$ resolution *IUE* spectra obtained through the $10'' \times 20''$ large aperture would collect most of red-shifted backscattered dust emission. Using the dust grain constants and size distribution described in Harper et al. (2001) and requiring that the scattering optical depth in the ultraviolet be $\tau_{\rm sca}^{uv} \leqslant 3$ to allow for the forward scattering phase function and dust absorption, e.g., Lefèvre (1992), we estimate that the circumstellar dust shell has V absorption optical depth of $\tau_{\rm abs}^{V} \leqslant 0.2$. Adopting an $M_V \geqslant -5.85$ for an M1-2 Iab star, which is consistent with the value for the M supergiant in the α Sco binary system, and an upper-limit of $A_V = 0.22$ we find for α Ori that a mean $\bar{V} \simeq 0.65$ implies that the distance is $\geqslant$180 pc, which is on the near end of our new distance range but on the far end of the *Hipparcos* distance.

5.3. The Life and Times

The kinematics of Betelgeuse are intriguing and not easily explained. The space motion is $[U', V', W'] = [-12.7, +0.5, +28.2$ km s$^{-1}]$ for a distance of 197 pc. The current galactic coordinates relative to the Sun are $[X, Y, Z] = [-182, -66, -31$ pc] and therefore projection of Betelgeuse's space motion back in time only takes the star farther from the galactic plane. The age of an early M supergiant with an initial mass of 20 $M_\odot$ is ∼10 Myr (Meynet & Maeder 2003) and Betelgeuse would have moved ∼290 pc farther from the galactic plane over that time interval. Projecting the star's space motion back in time for 10 Myr does not place it close to any likely star formation region for any adopted distance between 150 and 300 pc.

One possible explanation is that Betelgeuse has not followed its current space motion for all its life. If the space motion is projected backwards in time, 2.5 Myr ago Betelgeuse passed through the extensive Ori OB1a star-formation region. Briceñeno et al. (2005) find an age of 7–11 Myr for Ori OB1a depending on the evolutionary tracks used (7.4 Myr results from the Baraffe et al. (1998) tracks, while 10.7 Myr results from those of Siess et al. (2000)). One of the clearest subassociations within Ori OB1a is the 25 Ori group which has an age of 10 Myr and a distance of 330 pc (Briceño et al. 2007) and $[X, Y, Z] = [-292, -112, -104$ pc]. α Ori's projected path apparently does not intersect precisely with the 25 Ori group but the space motion for this group is not yet measured. However, the most likely formation scenario is that Betelgeuse is another runaway star from Ori OB1 (see, e.g., Hoogerwerf et al. 2000) and was originally a member of a high-mass multiple system within Ori OB1a.

Formation close to the far younger Orion Nebula Cluster (ONC, also known as Ori OB1d) is much less likely. The distance to the ONC has been measured from VLBA astrometry to be 389^{+24}_{-21} pc (Sandstrom et al. 2007) and 414 ± 7 pc (Menten et al. 2007). The space motion of the ONC is approximately $[U', V', W'] = [-11.0, -2.4, +1.1$ km s$^{-1}]$ (see Sandstrom et al. 2007) and its location is $[X, Y, Z] = [-322, -178, -129$ pc]. While the ONC lies more than 100 pc from the galactic plane, its motion orthogonal to the galactic plane is very small unlike the motion of Betelgeuse. Figure 4 shows a representation of Betelgeuse's position as a function of age in comparison with the young ONC and older Ori OB1 association.

6. CONCLUSIONS

Positions of Betelgeuse from high spatial resolution multi-wavelength VLA observations have lead to a reduction in the parallax, and an increased distance, as compared to that measured by *Hipparcos*. Our new proper motions are barely consistent with the latest *Hipparcos* solutions and the required *cosmic noise* suggests that systematic errors remain in the *Hipparcos* solution. By combining the *Hipparcos* and VLA positional data, the different kinds of systematic erros may result in a more robust result. In a sense, the derived distance of 200 pc is a balance between the 131 pc *Hipparcos* distance and the radio which tends towards 250 pc. Future new radio positions should lead to an improved astrometric solution.

It should be borne in mind that because the angular size of Betelgeuse is significantly greater than its parallax it is not an ideal target for parallax studies. However, the multiwavelength approach allows for checks on systematic errors arising from atmospheric phase corrections and unresolved stellar structures, and provides robust error estimates on the measured stellar positions. Understanding the systematic behavior of the non-fast-switched X-band declinations may allow further refinement of the parallax, and using X-band fast-switching may elucidate this matter. We plan to reobserved Betelgeuse at strategic epochs in order to refine the parallax.

The *Hipparcos* and VLA-*Hipparcos* distances both suggest that if the infrared arcs observed $7'$ from the star are indeed a wind-ISM bow shock then the surrounding ISM densities are not typical of local interstellar properties, and perhaps Betelgeuse's mass loss is plowing into the remnants of previous epochs of hot star mass loss. The new space motions suggest that Betelgeuse was not formed near the ONC, but more likely was a member of a high-mass multiple system within Ori OB1a.

We thank the referee for their careful review which materially improved this work. This research was supported by NASA under ADP grant NNG04GD33G (GMH) issued through the Office of Space Science, by NSF grant AST-0206367 (AB,GMH), and travel support by NRAO. We wish to thank C. Carilli and M. Claussen for their assistance in the planning and execution of the observations for VLA projects AH0778 and AH0824. We also thank S. Engle for his assistance.

Facilities: VLA, *Hipparcos*.

REFERENCES

Baraffe, I., Chabrier, G., Allard, F., & Hauschildt, P. H. 1998, A&A, 337, 403
Beasley, A. J., et al. 2002, ApJS, 141, 13
Bennett, P. D., Harper, G. M., Brown, A., & Hummel, C. A. 1996, ApJ, 471, 454
Bernat, A. P., Hall, D. N. B., Hinkle, K. H., & Ridgway, S. T. 1979, ApJ, 233, L135
Bessell, M. S. 2000, PASP, 112, 961
Blondin, J. M., & Koerwer, J. F. 1998, New Astron., 3, 571
Boboltz, D. A., Fey, A. L., Johnston, K. J., Claussen, M. J., de Vegt, C., Zacharias, N., & Gaume, R. A. 2003, AJ, 126, 484
Boboltz, D. A., Fey, A. L., Puatua, W. K., Zacharias, N., Claussen, M. J., Johnston, K. J., & Gaume, R. A. 2007, AJ, 133, 906
Briceño, C., Calvet, N., Hernández, J., Vivas, A. K., Hartmann, L., Downes, J. J., & Berland, P. 2005, AJ, 129, 907
Briceño, C., Hartmann, L., Hernández, J., Calvet, N., Vivas, A. K., Furesz, G., & Szentgyorgyi, A. 2007, ApJ, 661, 1119
Brown, A., & Harper, G. M. 2004, in IAU Symp. No. 219, ed. A. K. Dupree, & A. O. Benz, 646
Carilli, C. L., v & Holdaway, M. A. 1997, VLA Scientific Memo No. 173
Carpenter, K. G. 1984, ApJ, 285, 181
Chiavassa, A., Plez, B., Josselin, E., & Freytag, B. 2006, in Semaine de l'Astrophysique Francaise, SF2A-2006, ed. D. Barret, F. Casoli, G. Lagache, A. Lecavelier, & L. Pagani, 455
Dgani, R., van Buren, D., & Noriega-Crespo, A. 1996, ApJ, 461, 927
Dupree, A. K., Baliunas, S. L., Guinan, E. F., Hartmann, L., Nassiopoulos, G. E., & Sonneborn, G. 1987, ApJ, 317, L85

ESA 1993, The *Hipparcos* Input Catalogue, ESA SP-1136
ESA 1997, The *Hipparcos* and *Tycho* Catalogues, ESA SP-1200
Freytag, B., Steffen, M., & Dorch, B. 2002, Astron. Nachr., 323, 213
Fricke, W., Schwan, H., & Lederle, T. 1988, Veroeff. Astron. Rechen-Institut Heidelberg, No. 32, Fifth Fundamental Catalogue (FK5)
Frisch, P. C., Sembach, K., & York, D. G. 1990, ApJ, 364, 540
Goldberg, L. 1984, PASP, 96, 366
Guo, J. H., & Yi, Y. 2002, ApJ, 565, 559
Harper, G. M., & Brown, A. 2006, ApJ, 646, 1179
Harper, G. M., Brown, A., & Lim, J. 2001, ApJ, 551, 1073
Harper, G. M., Brown, A., Bennett, P. D., Baade, R., Walder, R., & Hummel, C. A. 2005, AJ, 129, 1018
Hoogerwerf, R., De Bruijne, J. H. J., & De Zeeuw, P. T. 2000, ApJ, 544, L133
Huggins, P. J. 1987, ApJ, 313, 400
Huggins, P. J., Bachiller, R., Cox, P., & Forveille, T. 1994, ApJ, 424, L127
Jones, H. S. 1928, MNRAS, 88, 660
Josselin, E., & Plez, B. 2007, A&A, 469, 671
Kovalevsky, J., et al. 1992, A&A, 258, 7
Keenan, P. C., & McNeil, R. C. 1989, ApJS, 71, 245
Kiss, L. L., Szabó, G. M., & Bedding, T. R. 2006, MNRAS, 372, 1721
Knapp, G. R., & Morris, M. 1985, ApJ, 292, 640
Johnston, K., de Vegt, C., & Gaume, R. 2003, AJ, 125, 3252
Lallement, R., Welsh, B. Y., Vergely, J. L., Crifo, F., & Sfeir, D. 2003, A&A, 411, 447
Lambert, D. L., Brown, J. A., Hinkle, K. H., & Johnson, H. R. 1984, ApJ, 284, 223
Lefèvre, J. 1992, A&A, 254, 274
Levesque, E. M., Massey, P., Olsen, K. A. G., Plez, B., Josselin, E., Maeder, A., & Meynet, G. 2005, ApJ, 628, 973
Lim, J., Carilli, C. L., White, S. M., Beasley, A. J., & Marson, R. G. 1998, Nature, 392, 575
Lindegren, L., et al. 1992, A&A, 258, 18
Ma, C., et al. 1998, AJ, 116, 516
Menten, K. M., Reid, M. J., Forbrich, J., & Brunthaler, A. 2007, A&A, 474, 515
Meynet, G., & Maeder, A. 2003, A&A, 404, 975
Mignard, F., & Froeschlé, M. 2000, A&A, 354, 732
Mozurkewich, D., et al. 2003, AJ, 126, 2502
Noriega-Crespo, A., van Buren, D., Cao, Y., & Dgani, R. 1997, AJ, 114, 837
Paresce, F. 1984, AJ, 89, 1022
Perrin, G., Ridgway, S. T., Coudé du Foresto, V., Mennesson, B., Traub, W. A., & Lacasse, M. G. 2004, A&A, 418, 675
Platais, I., et al., 2–3, A&A, 397, 997
Pourbaix, D., Platais, I., Detournay, S., Jorissen, A., Knapp, G., & Makarov, V. V. 2003, A&A, 399, 1167
Reid, M. J., & Menten, K. M. 1997, ApJ, 476, 327
Rowan-Robinson, M., Lock, T. D., Walker, D. W., & Harris, S. 1986, MNRAS, 222, 273
Sandstrom, K. M., Peek, J. E. G., Bower, G. C., Bolatto, A. D., & Plambeck, R. L. 2007, ApJ, 667, 1161
Sanford, R. F. 1933, ApJ, 77, 110
Schwan, H. 2001, A&A, 367, 1078
Siess, L., Dufour, E., & Forestini, M. 2000, A&A, 358, 593
Smith, M. A., Patten, B. M., & Goldberg, L. 1989, AJ, 98, 2233
Stothers, R. 1969, ApJ, 156, 541
Stothers, R., & Leung, K. C. 1971, A&A, 10, 290
Turner, D. G., Rohanizadegan, M., Berdnikov, L. N., & Pastukhova, E. N. 2006, PASP, 118, 1533
Uitenbroek, H., Dupree, A. K., & Gilliland, R. L. 1998, AJ, 116, 2501
van Altena, W. F., Lee, J. T., & Hoffleit, E. D. 1995, Yale Trigonometric Pallaxes (4th ed; Yale Univ. Obs.)
van Belle, G. T., et al. 1999, AJ, 117, 521
van Buren, D., & McCray, R. 1988, ApJ, 329, L93
van Leeuwen, F. 2007, *Hipparcos*, the New Reduction of the Raw Data (Dordrecht: Springer)
van Leeuwen, F., & Evans, D. W. 1998, A&AS, 130, 157
Walter, H. G., & Hering, R. 2005, A&A, 431, 721
Wasatonic, R., Guinan, E. F., & Engle, S. 2005, BAAS, 37, 1364
White, N. M. 1980, ApJ, 242, 646
Wilkin, F. P. 1996, ApJ, 459, L31